

Constitutive Model for Cyclic Behaviour of Cohesionless Sands

Mojtaba Rahimi, Dave Chan, Alireza Nouri

Department of Civil & Environmental Engineering, University of Alberta, Edmonton, AB, Canada.

Abstract

This paper presents a constitutive model for describing the stress-strain response of sands under cyclic loading. The model, formulated using the critical state theory within the bounding surface plasticity framework, is an upgraded version of an existing model developed for monotonic behavior of cohesionless sands. With modification of the hardening law, plastic volumetric strain increment and unloading plastic modulus, the original model was modified for simulating cyclic loading. The proposed model was validated against triaxial cyclic loading tests for Fuji River sand, Toyoura sand and Nigata sand. Comparison between the measured and predicted results suggests that the proposed modified model can capture the main features of cohesionless sands under drained and undrained cyclic loading.

1. Introduction

Classical plasticity is based on the concept of a single yield surface which is used to separate the elastic and plastic domains. Traditional plasticity provides a good description for the overall stress-strain behaviour of monotonic loading when no unloading occurs. However, it has some major drawbacks with regard to the simulation of cyclic loading. The most critical deficiency is that it provides a purely elastic response within the yield surface [Yu 2006]. The idealized stress-strain curve of Fig. 1 implies that large plastic strains are predicted by the model during primary loading, but during the subsequent unload-reload, only purely elastic strains within the yield surface are predicted. Additional plastic strain can occur only upon reloading to a stress state beyond the inception point of the stress reversal, point A' , and when the subsequent behaviour is identical to the case

that would have occurred as if there was no unloading [Chen and Han 2007]. This is not suitable for modeling the behaviour of soil under cyclic loading because in reality, all unload-reload cycles give rise to a gradual stockpile of plastic strain and energy dissipation [Khong 2004, Yu et al. 2007].

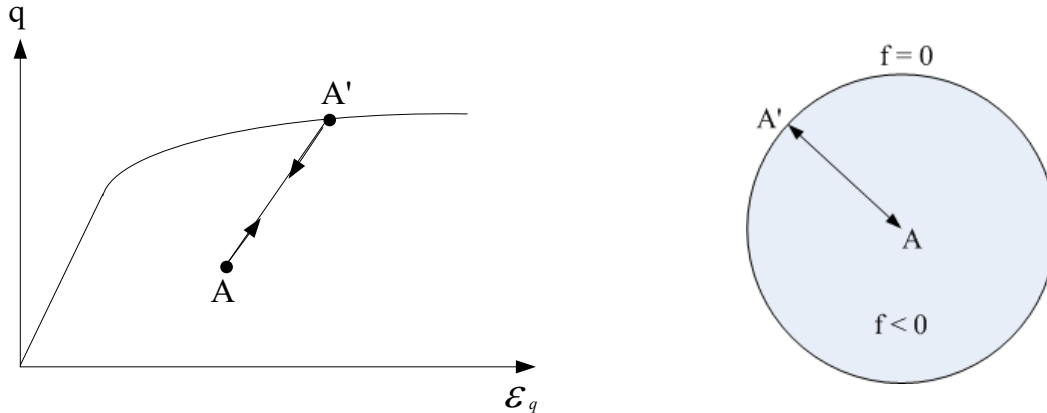


Fig. 1 Unloading and reloading from an elasto-plastic state: idealized stress-strain curve using traditional plasticity

Therefore, classical plasticity cannot replicate the non-linearity of the modulus, accumulation of plastic strain nor irrecoverable pore pressure generation during unloading and consequent reloading [Habte 2006, Yu 2006, Yang et al. 2011]. That is, it fails to duplicate complicated behaviour observed under cyclic loading conditions in the elasto-plastic range (i.e. cyclic plasticity), where stress reversal takes place frequently. This shortcoming of the traditional models was a turning point for the plasticity theory, which finally led to the development of alternative plasticity models [Reilly and Brown 1991, Chen 1994, Yu 2006].

Multi-surface and bounding surface plasticity are two mainstream approaches for modeling soil behaviour in response to cyclic loading (Reilly and Brown 1991, Habte 2006, Yu et al. 2007, Suebsuk et al. 2011, Yang et al. 2011). The theory of multi-surface or nested plasticity originally was introduced by Mroz (1967) and Iwan (1967) for metals, but immediately found applications in the modeling of geomaterials [Yu 2006, Suebsuk et al. 2011]. In general, however, multi-surface plasticity models are complicated due to the use of many sub-yield surfaces and the need to track the position and size of all yield surfaces in the stress space [Chen 1994]. This demands a considerable amount of computational resources for the

configuration of sub-yield and stress reversal surfaces. There are substantial challenges with increasing the number of yield surfaces in a model, making the model computationally very demanding and numerically more unstable [Chen 1994, Suebsuk et al. 2011, Yang et al. 2011]. Bounding surface plasticity was introduced to address some of the numerical shortcomings of multi-surface plasticity. For example, there is no need to track the locations and sizes of all the active yield surfaces in the bounding surface theory since yielding is assumed to be continuous inside the bounding surface. Hence, the location of the two surfaces effectively describes the distribution of all intermediate loading surfaces, thus references to them are not essential [Yu 2006]. Dafalias and Popov (1975, 1977) and Krieg (1975) independently proposed the bounding surface plasticity concept for the first time using kinematic hardening. Many similar models have been introduced later specially for clays [for example see Mroz et al. 1979, Pastor et al. 1985, Zienkiewicz et al. 1985, Al-Tabbaa 1987, Stallebrass 1990, McDowell and Hau 2004]. Dafalias and Herrmann (1982) and Dafalias (1986) originally introduced the radial mapping formulation of the bounding surface theory. The radial mapping scheme has been adopted in many models that were later proposed within the bounding surface plasticity framework [for example see Bardet 1986, Crouch et al. 1994, Ling et al. 2002, Khong 2004, Russel and Khalili 2004, Khalili et al. 2005, Yu et al. 2007, Yang et al. 2008, Suebsuk et al. 2011, Kan et al. 2014]. This paper presents a specific version of the bounding surface plasticity, which does not incorporate the radial mapping formulation. That is, unlike conventional bounding surface plasticity in which the plastic modulus is expressed as the summation of the additive and bounding surface plastic moduli, the plastic modulus is stated only as a function of that of the loading surface. This is similar to Imam and Chan's (2008) approach for modelling cyclic loading.

2. Brief overview of the original model

The detailed formulation of the original model can be reviewed in Imam (1999) and Imam et al. (2005). A brief overview is provided here.

The yield function is expressed as:

$$f = (\eta - \alpha)^2 - M_\alpha^2 \left(1 - \sqrt{\frac{p}{p_c}} \right) = 0 \quad (1)$$

$$M_\alpha^2 = (5M_p - \alpha)(M_p - \alpha) \quad (2)$$

where η is the stress ratio, M_p is the stress ratio at the peak of the undrained effective stress path (UESP), p is the mean effective stress, α is a scalar constant whose magnitude is non-zero only for anisotropically consolidated sands and p_c is the preconsolidation stress which controls the size of the yield surface.

Note the parameter M_p determines the stress conditions at which the cap and the front portion of the yield surface are separated from each other. It is also used to evaluate the stress ratio at the peak of the yield surface. This is consistent with early claims that in loose sands, the stress ratio at the peak of the yield surface is very close to the stress ratio at the peak of UESP [Imam 1999]. M_p is evaluated for compression and extension, respectively, as follows:

$$M_{p,c} = \frac{6 \sin \varphi_{p,c}}{3 - \sin \varphi_{p,c}} \quad (3)$$

$$M_{p,e} = \frac{6 \sin \varphi_{p,e}}{3 + \sin \varphi_{p,e}} \quad (4)$$

in which $\varphi_{p,c}$ and $\varphi_{p,e}$ are the friction angles at the point of peak shear stress in the triaxial compression and triaxial extension tests, respectively. They can be calculated by:

$$\sin \varphi_{p,c} = \sin \varphi_\mu - k_p \psi_p \quad (5)$$

$$\sin \varphi_{p,e} = \sin \varphi_\mu - k_p \psi_p - a_p \quad (6)$$

where $\psi_p = e - e_p$ is the state parameter at the peak in which e is void ratio, and e_p is the critical state void ratio which is evaluated at mean effective stress corresponding to M_p (i.e. at $p = p_p$), φ_μ is the friction angle associated with $\psi_p = 0$ in triaxial compression and is close to the interparticle friction angle and k_p and a_p are model parameters. Experimental observations which support dependency

of M_p on void ratio and the state parameter at the peak can be found in Imam et al. (2002).

When the stress path is at the peak of UESP, it is found from equation (1) that $p_p = 0.64 p_c$ for isotropically consolidated sands regardless of void ratio and confining pressure at consolidation. This relationship is similar to Ishihara (1993) relationship, who observed that the ratio of mean normal stress at the peak of UESP to that at consolidation is constant. By conducting undrained tests on sands consolidated to different mean normal stresses and void ratios, he obtained ratios of 0.61 and 0.63 for a clean and silty sand, respectively [Imam et al. 2005].

Isotropic nonlinear elasticity is assumed for the model. The shear and bulk moduli are calculated from the following equations:

$$G = G_a \frac{(2.973 - e)^2}{1 + e} \left(\frac{p}{p_{atm}} \right)^n \quad (7)$$

$$K = K_a \frac{(2.973 - e)^2}{1 + e} \left(\frac{p}{p_{atm}} \right)^n \quad (8)$$

in which G_a and K_a are reference elastic moduli accounted as material parameters and p_{atm} is the atmospheric pressure. A value of 0.5-0.55 is usually used for n , depending on the type of sand.

Following the work of Wood (1990) and Manzari and Dafalias (1997), the stress-dilatancy relationship is defined as:

$$D = A(M_{PT} - \eta) \quad (9)$$

$$A_c = \frac{9}{9 + 3M_{PT,c} - 2M_{PT,c}\eta} \quad (10)$$

$$A_e = \frac{9}{9 - 3M_{PT,c} - 2M_{PT,c}\eta} \quad (11)$$

where

$$\sin \varphi_{PT,c} = \sin \varphi_{CS} + k_{PT} \psi_s \quad (12)$$

$$\sin \varphi_{PT,e} = \sin \varphi_{CS} + k_{PT} \psi_s + a_{PT} \quad (13)$$

in which M_{PT} is the phase transformation stress ratio, φ_{CS} is the critical state friction angle, $\psi_s = e - e_{CS}$ is the state parameter [Been and Jefferies 1985, Jefferies 1993], e_{CS} is the critical void ratio and k_{PT} and a_{PT} are both model parameters. Similar to how M_p is calculated using $\sin\varphi_p$ under triaxial compression and extension conditions, M_{PT} under compression and extension conditions is obtained from $\sin\varphi_{PT}$. Equation (12) and (13) are similar to the Manzari and Dafalias (1997) relationship [Imam et al. 2005]. Note that the phase transformation concept was originally introduced by Tatsuoka and Ishihara (1974).

Hardening in this model depends on the proximity to the critical state, in contrast to conventional critical state models which relate the size of the yield surface to void ratio [Jefferies 1993]. Pure size shear hardening law is stated as:

$$\frac{\partial p_c}{\partial \varepsilon_q^p} = \frac{hG_{ini}}{(p_f - p_c)_{ini}} (p_f - p_c) \quad (14)$$

in which h is a material parameter, p_f is the failure mean effective stress and $(p_f - p_c)_{ini}$ is the initial value of $(p_f - p_c)$ at the end of consolidation and prior to shearing. Calculation of M_f is based on $\sin\varphi_f$ which itself is obtained by:

$$\sin\varphi_f = \sin\varphi_{CS} - k_f\psi_s \quad (15)$$

where k_f is a material parameter.

3. A bounding surface model for the cyclic response of sand

The major components of the proposed two-surface model are elasticity, stress-dilatancy relationship, loading surface and bounding surface, stress-strain relationships and loading criterion. They are briefly discussed here.

3.1 Elasticity

Isotropic nonlinear elasticity adopted for the original model is retained for simplicity.

3.2 Stress-dilatancy relationship

The absolute value of the stress ratio $|\eta|$ is applied in the formula of the stress-dilatancy of the original model rather than the stress ratio η .

3.3 Loading surface and bounding surface

The loading surface is expressed as:

$$f = \left(\frac{q - q_a}{p - p_a} - \alpha \right)^2 - M_\alpha^2 \left(1 - \sqrt{\frac{p - p_a}{p_c}} \right) = 0 \quad (16)$$

where p_a and q_a are components of kinematic hardening tensor which evolves with plastic deformation. This definition of the loading surface suggests that p_a must always be smaller than p .

The loading surface during the first loading time is supposed to be identical to that of the original model, meaning the kinematic hardening tensor originally lies at the origin of the coordinate system.

The bounding surface is supposed to have the same shape as the loading surface for simplicity. Thus, the bounding surface is expressed as:

$$F = \left(\frac{\bar{q} - \bar{q}_a}{\bar{p} - \bar{p}_a} - \alpha \right)^2 - M_\alpha^2 \left(1 - \sqrt{\frac{\bar{p} - \bar{p}_a}{\bar{p}_c}} \right) = 0 \quad (17)$$

The superimposed bar denotes variables for the bounding surface. The size of the bounding surface is determined by \bar{p}_c .

The bounding surface provides an exterior limit for stress space since a stress state outside the bounding surface has no physical meaning. The bounding surface always encircles the loading surface, may touch it tangentially at a point or even becomes identical with it, but never intersects it [Chen 1994, Vermeer and Borst 1984, Chen and Han 2007]. Therefore, to ensure that the current stress state will not cross the bounding surface, the initial ratio of size of the two surfaces ($\bar{p}_c/p_c > 1$) is kept constant during the shearing process. The initial size of the loading and bounding surfaces at the start of shearing is considered to be equal to the hydrostatic pressure and failure mean effective pressure, respectively. It is also assumed that the components of the kinematic hardening tensor always coincide for the two

where c_1 and c_2 are model constants, $\dot{\varepsilon}_p^p$ and $\dot{\varepsilon}_q^p$ are plastic volumetric and deviator strain increments and \dot{p} is the accumulative plastic strain increment which is defined as:

$$\dot{p} = \sqrt{\frac{2}{3} \left(\frac{1}{3} \dot{\varepsilon}_p^p + \dot{\varepsilon}_q^p \right)^2 \left(2 \left(\frac{1}{3} \dot{\varepsilon}_p^p - \frac{1}{2} \dot{\varepsilon}_q^p \right)^2 \right)} \quad (20)$$

p_α and q_α are components of the kinematic hardening tensor which are defined as:

$$p_\alpha = \frac{\alpha_{11} + 2\alpha_{33}}{3} \quad (21)$$

$$q_\alpha = \alpha_{11} - \alpha_{33} \quad (22)$$

Note that the second term on the right side of equations (18) and (19) represents a nonlinear term for the proposed kinematic hardening model, while the first part is similar to Prager's linear kinematic hardening rule.

3.4 Stress-strain relationships

Constitutive relationships are governed by the following equations in accordance with standard incrementally linear stress-strain relationships:

$$\dot{p} = K \left(\dot{\varepsilon}_p - LD \text{sign}(m_p) \right) \quad (23)$$

$$\dot{q} = 3G \left(\dot{\varepsilon}_q - \sqrt{2/3} L \text{sign}(m_q) \right) \quad (24)$$

where K and G are bulk and shear elastic moduli, D is the dilatancy rate, L is the normalized plasticity multiplier and m_p and m_q are components of the unit normal to the plastic potential surface which can be obtained using the dilatancy relationship.

The parameter L is determined from the following relationship:

$$L = \frac{KR\dot{\varepsilon}_p + \sqrt{6}G\dot{\varepsilon}_q}{H_n + KR D + 2G} \quad (25)$$

$$R = \sqrt{\frac{2}{3} \frac{\partial f}{\partial p} \frac{\partial f}{\partial q}} \quad (26)$$

$$\frac{\partial f}{\partial p} = \frac{-2}{p - p_a} \left[\left(\frac{q - q_a}{p - p_a} \right)^2 - \alpha \left(\frac{q - q_a}{p - p_a} \right) \right] + \frac{M_\alpha^2}{2\sqrt{p_c(p - p_a)}} \quad (27)$$

$$\frac{\partial f}{\partial q} = \frac{2}{p - p_a} \left(\frac{q - q_a}{p - p_a} - \alpha \right) \quad (28)$$

$$m_q = \frac{1}{\sqrt{1 + D^2}} \quad (29)$$

$$m_p = \begin{cases} \frac{tD}{\sqrt{1 + D^2}} & D \geq 0 \\ \frac{-tD}{\sqrt{1 + D^2}} & D < 0 \end{cases} \quad (30)$$

where $t = 1$ for compressive loading and $t = -1$ for extensive loading. The definition of m_p based on the sign of the dilatancy rate for a given loading direction enables the proposed model to capture phase transformation under undrained cyclic loading. Also, different signs of m_p for compression and extension under a given dilatancy rate enables the model to capture the prevalent volumetric contraction observed during the cyclic loading of loose sands.

Components of the unit vector to the plastic potential surface for unloading are assumed to be related to those defined already as follows:

$$m_{p,u} = -m_p \quad (31)$$

$$m_{q,u} = m_q \quad (32)$$

Applying consistency condition for a combined isotropic shear and kinematic hardening law and ignoring shape hardening, the normalized plastic modulus can be calculated for triaxial condition using:

$$H_n = -\sqrt{\frac{2}{3}} \frac{1}{\left| \frac{\partial f}{\partial q} \right|} \frac{\partial f}{\partial p_c} \frac{\partial p_c}{\partial \varepsilon_q^p} + H_n^{kinematic} \quad (33)$$

$$H_n^{kinematic} = R \left(\frac{2}{9} c_1 D - c_2 p_\alpha \sqrt{\frac{2}{9} D^2 + 1} \right) + c_1 - c_2 u_Q q_\alpha \sqrt{\frac{2}{9} D^2 + 1} \quad (34)$$

in which

$$\frac{\partial f}{\partial p_c} = \frac{-M_\alpha^2}{2p_c} \sqrt{\frac{p - p_a}{p_c}} \quad (35)$$

$$u_Q = \frac{\frac{\partial f}{\partial q}}{\left| \frac{\partial f}{\partial q} \right|} \quad (36)$$

H_n for unloading is supposed to be related to loading as follows:

$$\frac{H_{n,u}}{H_n} = R_u \sqrt{\frac{p}{0.01p_{atm}}} |\eta| \quad (37)$$

The application of the stress ratio in the definition of the unloading plastic modulus results in a gradual decrease in the value of $H_{n,u}$ due to a decreasing trend in the stress ratio with progress in unloading. This implies that more plastic deformation occurs with the advancement of unloading, which is in line with experimental observations.

R_u is a positive value greater than one. This implies that the unloading-induced plastic strain increment is smaller than the loading induced plastic strain increment because a larger plastic modulus leads to a smaller plasticity multiplier and ultimately a smaller plastic strain increment.

A simple analysis of the definition of the plastic deviator strain increment reveals that the total, elastic and plastic deviator strain increments always have the same sign. They are all positive under compressive loading or extensive unloading. However, negative values are predicted for all of them under compressive unloading or extensive loading. Note that the sign of the normalized plasticity multiplier (L) is positive under compressive loading or extensive unloading. It, however, is negative for compressive unloading or extensive loading. In general, L is positive when the total deviator strain increment is positive and vice versa. Prediction of a negative plasticity multiplier for some loading conditions originates from the adopted formulation in this bounding surface plasticity model. It is assumed in this model that the current stress state always lies on the loading surface regardless of the loading type or stress path position. Therefore, elastoplastic deformation is predicted by the model throughout the shearing process from start to the end of loading/unloading process. To fulfill this condition, the loading surface should be obliged to pass through the current stress state at all times and loading

conditions using the consistency condition. This enforcement causes the normalized plasticity multiplier to become negative in some loading conditions. The classical plasticity principle which considers a zero value for non-positive plasticity multipliers is not followed here clearly. If this restriction is forced to be satisfied, the loading surface can not pass through the current stress state at all loading conditions and times. Moreover, a purely elastic response will be predicted by the model for some loading conditions and times if this restriction is imposed on the model formulation.

3.5 Loading criterion and loading direction

$$\dot{f} = \frac{\partial f}{\partial p} \dot{p} + \frac{\partial f}{\partial q} \dot{q} \quad (38)$$

Positive values for \dot{f} signify loading, and negative values denote unloading.

The direction of loading can be determined either by the sign of the deviator stress or deviator part of the unit normal to the loading surface. Values for q and n_q are positive for compressive loading and negative for extensive loading.

4. Performance of the proposed bounding surface model

The proposed model was used to predict the behaviour of several two-way drained and undrained cyclic triaxial tests on cohesionless sands. The test data were gathered from the literature. Material parameters and their assigned values are presented in Table 1.

Table 1 Material parameters used for calibration of Fuji River sand, Toyoura sand and Nigata sand

Parameter	Fuji River sand	Toyoura sand	Nigata sand
k_p	1.5	1	1.5
φ_μ	24	21	21
a_p	0.15	0.15	0.15
φ_{cs}	31	31	28
k_{pT}	1.25	0.25	1.25
a_{pT}	0.10	0.15	0.10
G_a	5e6	5e6	5e6
K_a	8e6	8.5e6	8.5e6
h	1	1	1
k_f	0.75	0.75	0.75
c_1	5e6	0.5e6	5e6
c_2	500	500	500
R_u	5	5	5
$e_{cs} (p \text{ in MPa})$	$-.0063477p^3 + .0367p^2$ $-.11991p + 0.74$	$-.0063477p^3 + .0367p^2$ $-.11991p + .92548$	$-.0063477p^3 + .0367p^2$ $-.11991p + 0.76$

k_p , φ_μ , a_p , φ_{cs} , k_{pT} , a_{pT} , G_a , K_a , h , k_f , and e_{cs} vs. p are model parameters of the original model. Methods of determination of parameters of the original model have been given in Imam et al. (2005). The parameter R_u is determined by fitting model predictions to unloading part of experimental data. A smaller value of R_u leads to a softer unloading response and a larger unloading-induced plastic strain increment and vice versa. The parameters c_1 and c_2 determine contribution of anisotropic/kinematic hardening in the combined isotropic -anisotropic/mixed hardening law. The larger difference between c_1 and c_2 results in the higher contribution of the anisotropic hardening to the overall hardening. The constants c_1 and c_2 may be determined from stress-strain curve of the uniaxial tests [Araujo 2002, Dunne and Petrinic 2006].

4.1 Drained cyclic loading test on Fuji River sand

Fig. 3 shows the predictions of the proposed bounding surface model for drained cyclic tests conducted by Tatsuoka and Ishihara (1974) on Fuji River sand. The test

was performed on a medium dense sample of Fuji River sand with an initial void ratio and constant confining pressure equal to 0.74 and 200 *KPa*, respectively. The test was carried out using cyclic axial loads with increasing stress amplitude in successive cycles. Progressive contraction of sand with cyclic loading was captured by the model. Fig. 3 shows that the continuous increases of shear strain and stress ratio with the continuation of cyclic loading were reproduced in both the compression and extension sides. The model predicted the first clear dilative response in the extension side of the fourth cycle at a point, which has almost the same stress ratio, but slightly higher volumetric strain compared to those of the measured values. Dilative response, however, was anticipated on the compression side for the last cycle, while experimental observations suggest that it first occurs on the extension side. Overall, the difference between the observed and predicted volumetric strain at any given stress ratio in Fig. 3 is increased with increase in the number of cycles. That is, the discrepancy has accumulated during successive cycles which has led to the larger differences between the actual and predicted behavior. As mentioned, the model has predicted that the material undergoes the maximum capacity for compression on the compressive side of the last cycle which is not in line with the observed response. Hence the difference between the actual and predicted volumetric strain increases further in the last cycle. The reason is that the observed response shows further compaction (before the material experiences dilation in the extensive side of the last cycle) while the model has predicted dilative response which has resulted in a decrease in the value of the predicted volumetric strain. In terms of the formulation of the model, prediction of the premature phase transformation by the model implies that the predicted compressive phase transformation stress ratio for the last cycle at the given stress ratio is smaller than the actual one during the physical experiment. That is, the predicted stress ratio exceeds the predicted phase transformation stress ratio on the compressive side of the last cycle which leads to change of behavior from compressive to dilative.

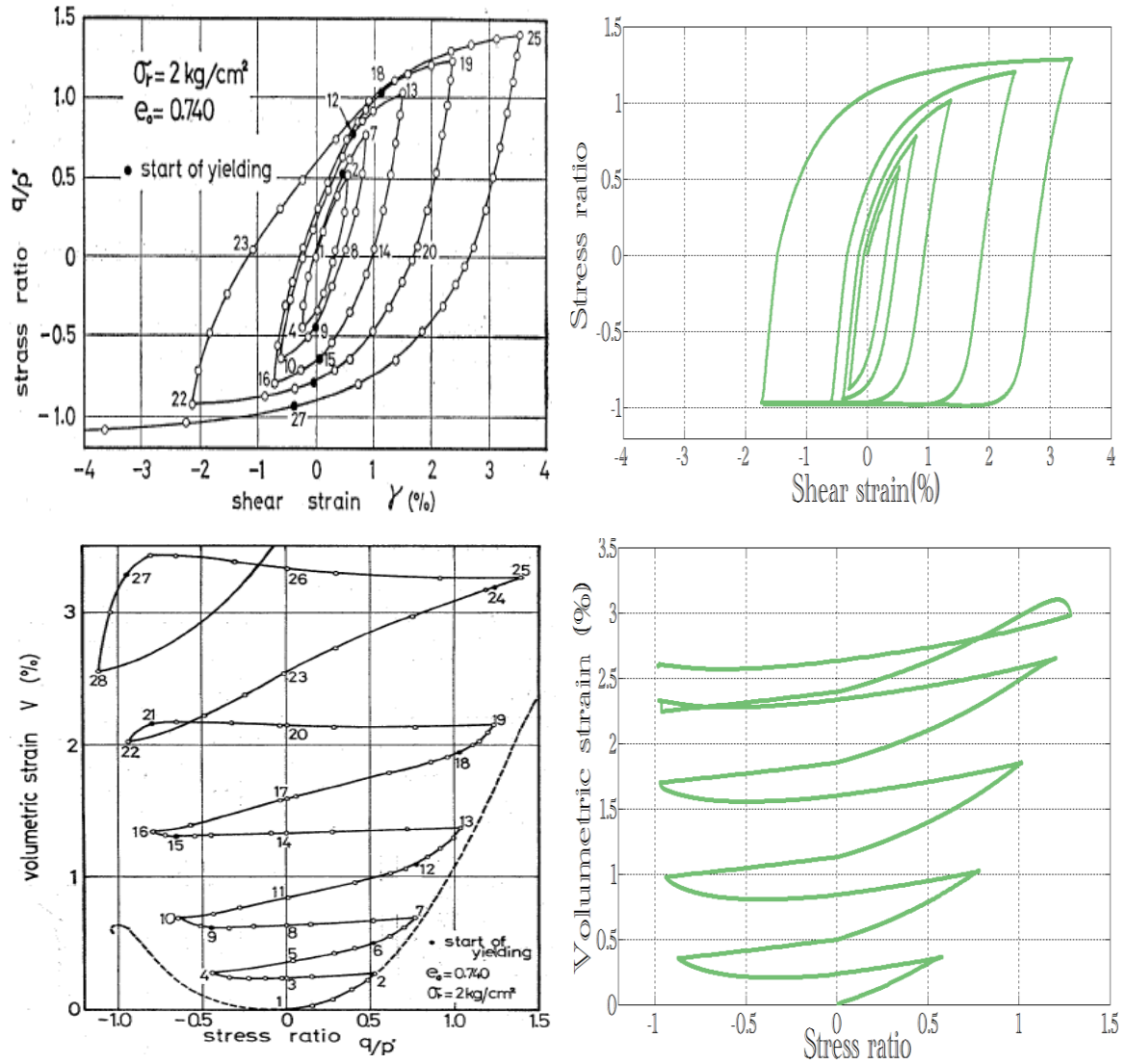


Fig. 3 Measured and predicted response of Fuji River sand during drained cyclic loading

4.2 Drained and undrained cyclic loading tests on Toyoura sand

Several two-way cyclic tests were conducted by Pradhan et al. (1989) on Toyoura sand. The sample used in Pradhan et al. (1989) consisted of quartz with angular to sub-angular particles [Ling and Yang 2006]. Drained cyclic tests on Toyoura sand were carried out under a constant p stress path. This stress path can be modeled by imposing a zero elastic volumetric strain increment, making the total volumetric strain equal to plastic volumetric strain. Figs. 4 to 6 show the results of the cyclic tests on Toyoura sand.

A reasonable agreement between the predicted and measured values of increasing amplitude of the stress ratio and shear strain during successive cycles can be found in Fig. 4. The successive softening and stiffening of the sample in the course of loading and unloading stages of cyclic loading are captured as well. However, the stronger dilative behaviour in the compressive side of the third cycle is predicted compared to the measured one.

Fig. 5 shows the constant p stress path during which the amplitude of shear strain decreases with the number of loading cycles and tends to approach a steady value. As observed, the trend and values of the shear strain and also the stress ratio have been captured by the model. The initial compression accompanied by subsequent expansion is captured by the model as well. However, the predicted tendency of the soil for dilation in compressive side of the successive cycles is stronger than the measured behaviour. This implies that the phase transformation surface is placed in a smaller q for a given p in the numerical model in comparison with the physical experiment. Thus, the predicted stress path reaches the phase transformation surface sooner than the experiment.

Fig. 6 displays triaxial undrained cyclic test on a saturated loose sample of Toyoura sand. The model predictions capture the stress-shear strain and the associated stress path during the constant deviator stress amplitude cycles ($q = \pm 25 \text{ KPa}$) very well. In particular, the model captures the progressive reduction in the mean effective stress, the ultimate deviator stress and also occurrence of the phase transformation in the extension side with reasonable accuracy. However, the stress path after the occurrence of the phase transformation (i.e. cyclic liquefaction) is not in very good agreement with the measured stress path. That is, the smaller reduction of the mean effective stress was predicted due to underestimation of excess pore pressure, which itself is directly linked to the magnitude of the volumetric strain increment. As it will be discussed later, accurate prediction of pore pressure generation after failure of the soil caused by cyclic liquefaction requires new formulation due to the dynamic nature of the hydromechanical process.

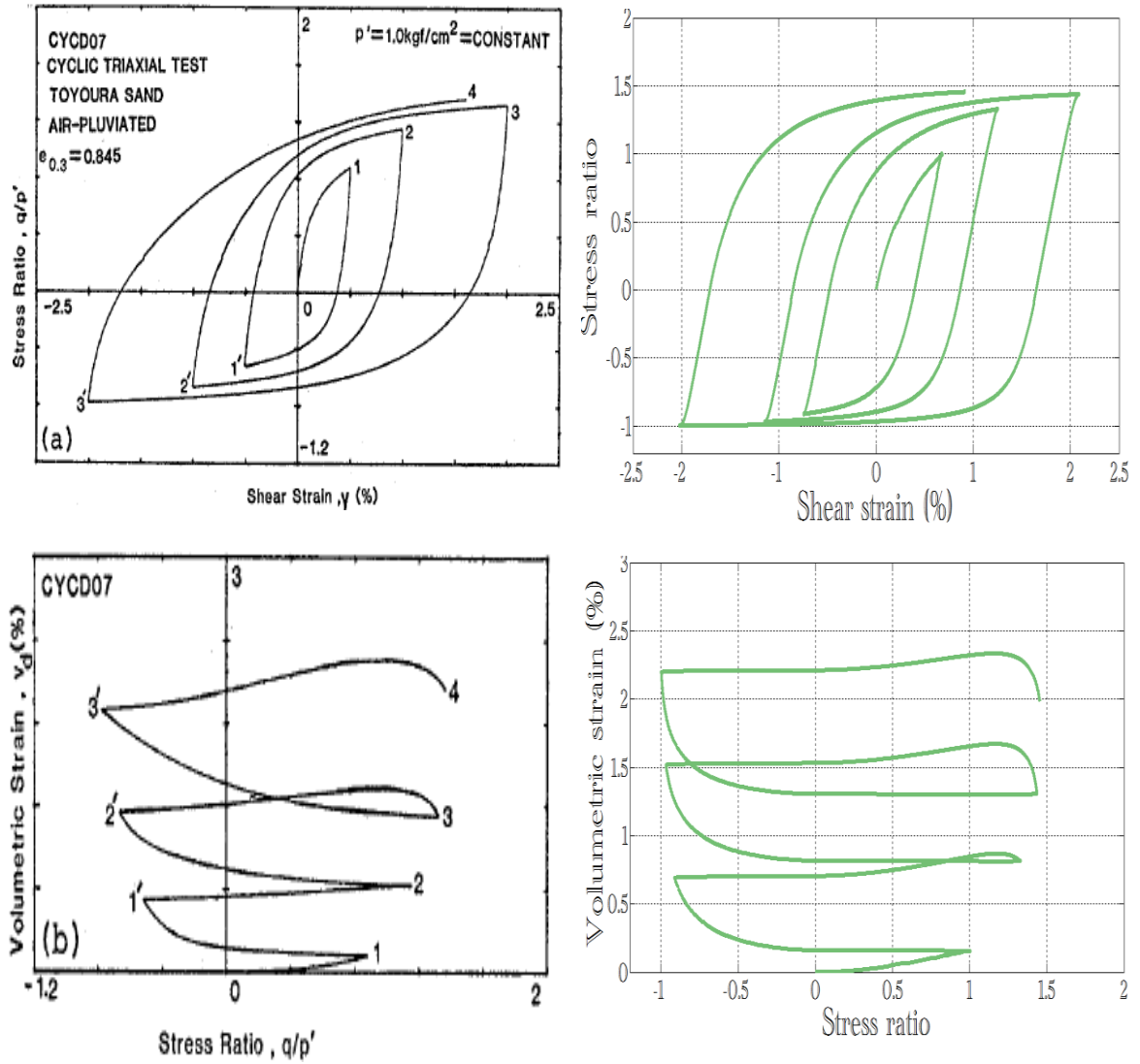


Fig. 4 Measured and predicted response of Toyoura sand during drained cyclic loading with an initial void ratio of 0.845 and confining pressure of 98 kPa

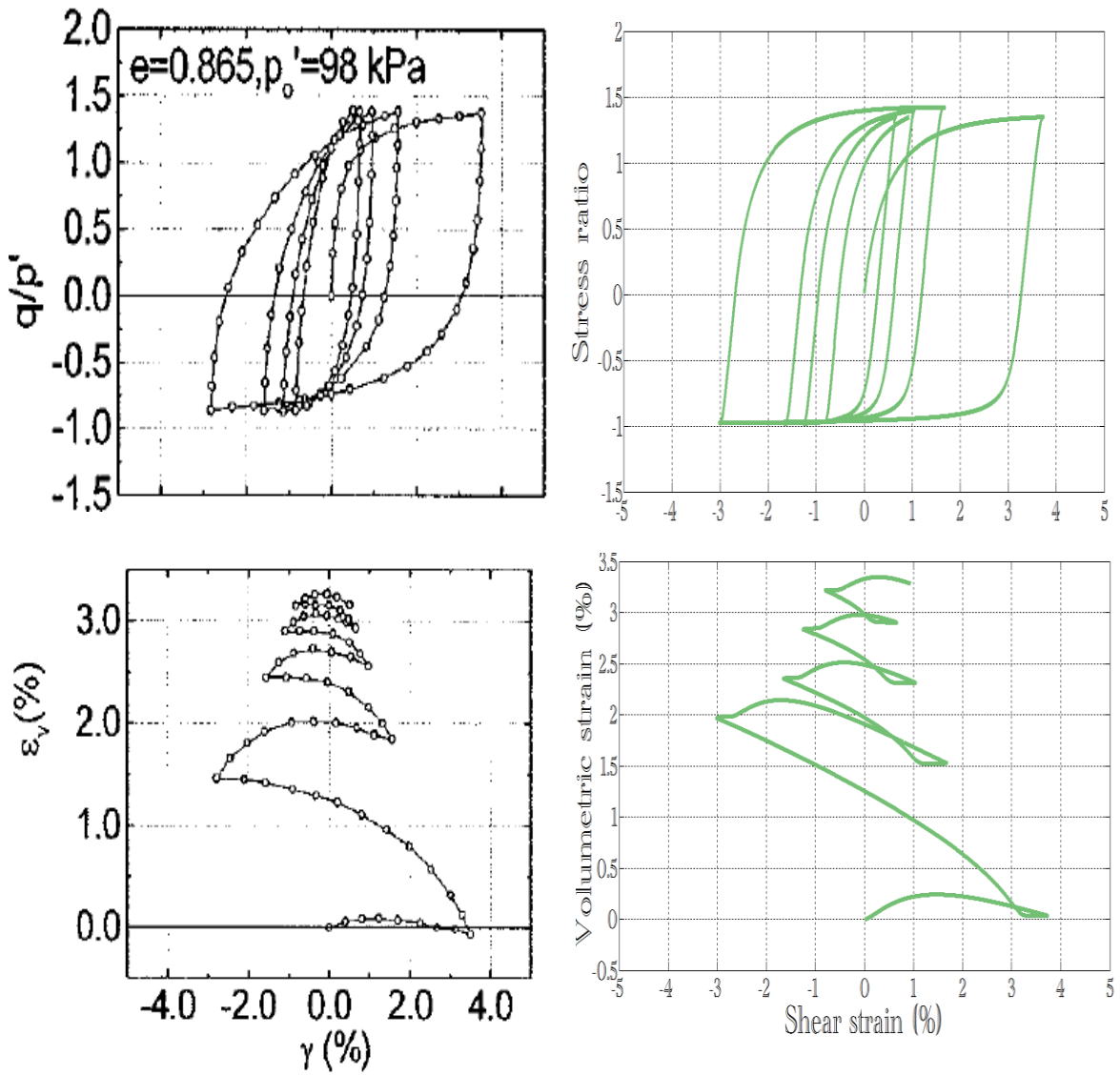


Fig. 5 Measured and predicted behaviour of Toyoura sand during drained cyclic loading with an initial void ratio of 0.865 and confining pressure of 98 kPa

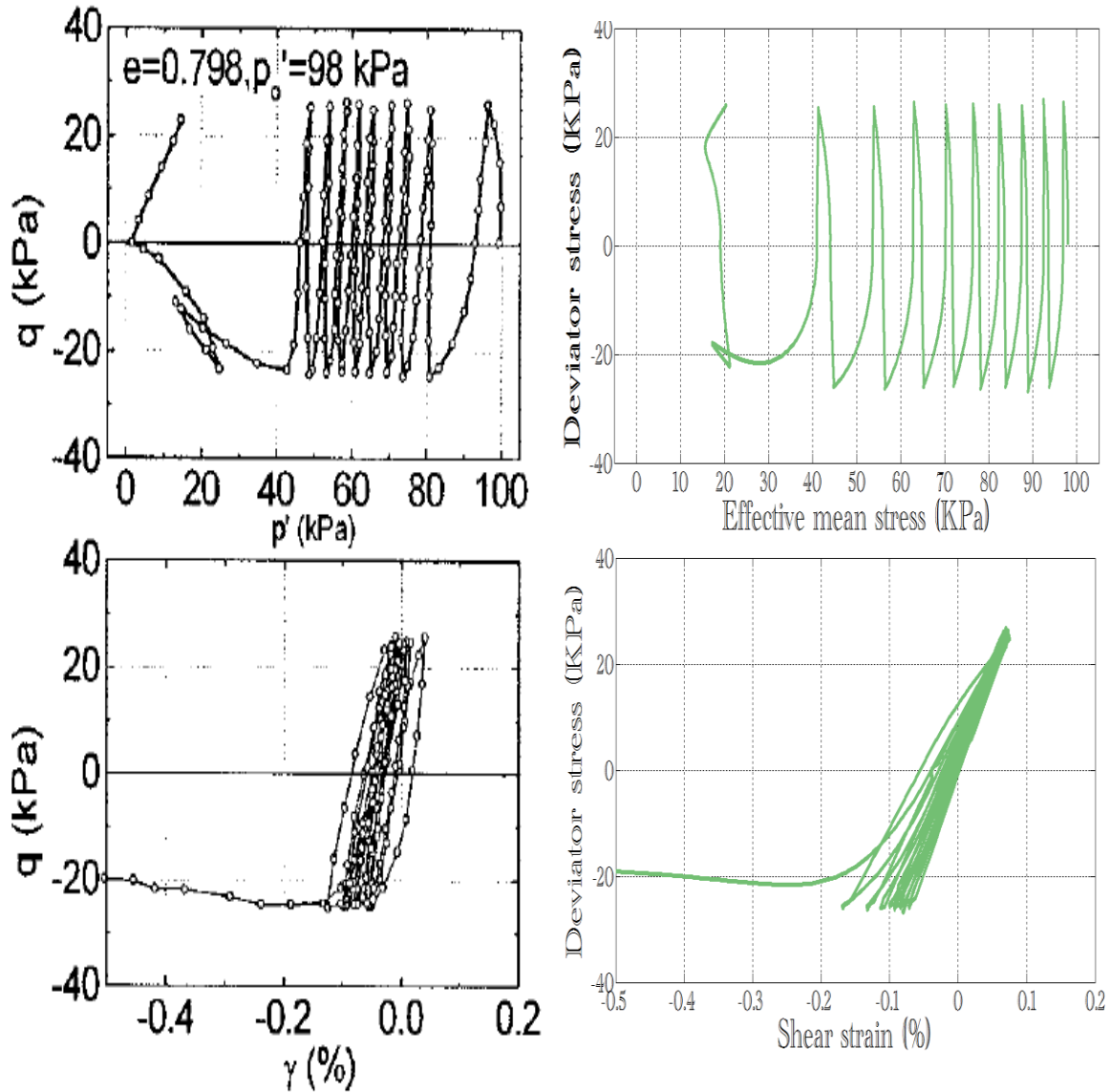


Fig. 6 Measured and predicted response of Toyoura sand during undrained cyclic loading with an initial void ratio of 0.798 and confining pressure of 98 kPa

4.3 Undrained cyclic loading test on Nigata sand

Fig. 7 plots the results of triaxial undrained stress-controlled cyclic loading test conducted by Ishihara et al. (1975) on a saturated sample of Nigata sand. During the initial cycles, the deviator stress-shear strain loops are almost vertical since very small shear strains/axial strains are developed. When the stress path reaches the phase transformation surface (i.e. cyclic liquefaction), the soil experiences a temporary constant volume phase by remaining on the phase transformation surface for a short time. This behaviour is accompanied by a constant q stress path and large

amounts of deformation. Decrease in p and large shear deformation without considerable increase in shear stress are common features of cyclic liquefaction and cyclic mobility [Lenart 2008]. Temporary steady-state behaviour ends as the stress path leaves the phase transformation surface resulting in dilative behaviour. Consequently, negative pore pressure develops and the mean effective stress increases. The contractive behaviour and positive pore pressure develops once more with stress reversal leading to decrease in the mean effective stress. The stress path hits the phase transformation surface in the compression side causing dilative behaviour and negative pore pressure development resulting in an increase in the mean effective stress. These fluctuations between the contractive and dilative behaviour cause the sand to continuously weaken (liquefy) and strengthen (densify) which indicates strong dilative response after the soil liquefies [Li and Ming 2000, Elgamal et al. 2003, Querol and Blázquez 2006, Lenart 2008, Orense and Pender 2012].

The proposed model captures the nearly vertical stress-strain behaviour and continuous reduction in mean effective stress in the initial constant deviatoric stress amplitude cycles ($q = \pm 75 \text{ KPa}$) fairly well. It also predicts cyclic liquefaction with reasonable accuracy at a stress point which has almost the same deviatoric stress and mean effective stress compared to those of the experiment. However, smaller shear deformations (i.e. stiffer response) were predicted by the model after the phase transformation, which has been shown by stress path 22-23. Also the reduction in the mean effective stress for stress path 23-24 is underestimated by the model because of the underestimation of the excess pore pressure. Consequently, the stress path reaches the phase transformation surface in the compression side at a stress point with greater deviatoric stress and the mean effective stress compared to the measured values. These discrepancies in matching the flowing behaviour continue during stress path 25-28, which has not been shown. The source of these differences originates from the fact that post-liquefaction behaviour is associated with very quick changes in pore pressure and plastic deformation [Yu et al. 2007]. Calculation of pore pressure development during the post-liquefaction phase needs special considerations. The rapid and large changes of the hydro-mechanical

properties by cyclic liquefaction can be captured by models which have been formulated for the earthquake type loading [Querol and Blázquez 2006, Yu et al. 2007, Lenart 2008]. The model can predict the successive phase transformations after point No. 25 (which have not been shown). However, these phase transformations occur with (very) small increment/decrement in the mean effective stress. This is due to underestimation of the pore pressure generation and plastic deformation. That is, a behavior similar to that of the cyclic mobility is predicted by the model rather than the cyclic liquefaction. Hence, the model cannot capture zero mean effective stress (i.e. fully free flow) which has obtained during the physical experiment.

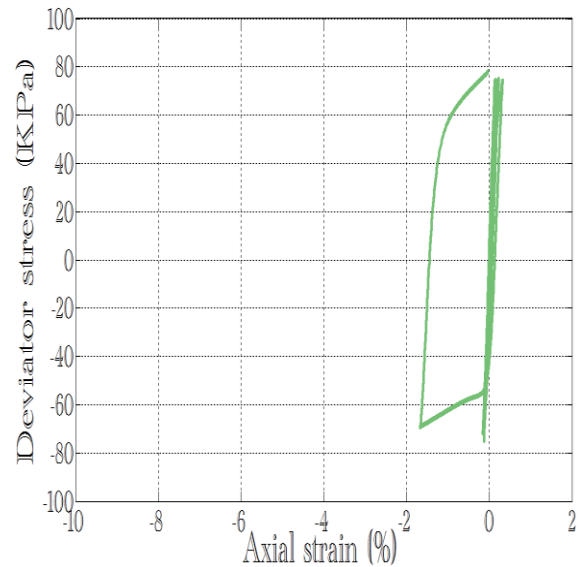
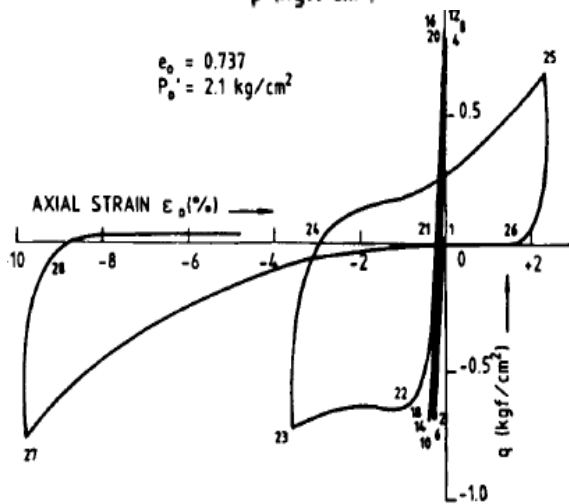
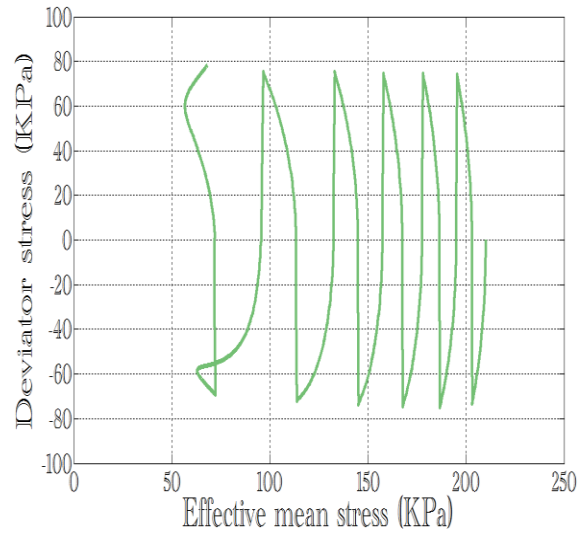
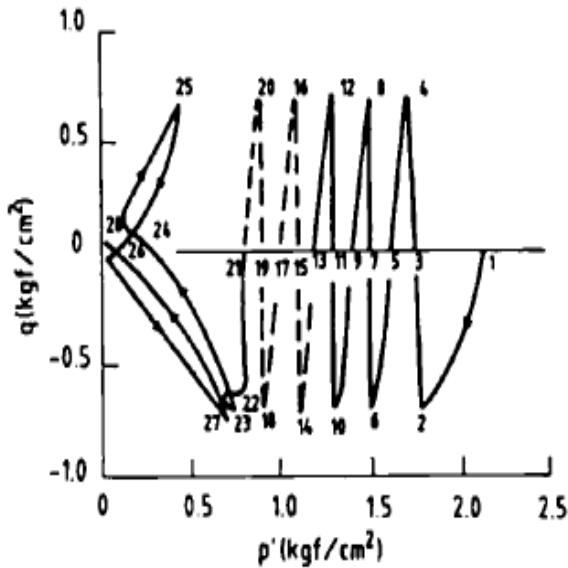


Fig. 7 Measured and predicted response of Nigata sand during undrained cyclic loading

5. Conclusion

A critical state constitutive model has been presented for cohesionless sands under cyclic loading within the framework of the bounding surface plasticity theory. Constitutive behavior of sand under different densities and pressures is captured in the proposed model by virtue of its dependency on the state parameter. Also due to indirect dependency of the flow rule on the state parameter, void ratio/density and pressure dependency is included indirectly in the dilatancy rate too.

Predictions of the proposed model for cyclic loading are in reasonable agreement with experimental measured data. The main characteristics of sand behaviour in response to cyclic loading have been captured fairly well. It, however, appears that if the definition of the pore pressure generation and plastic modulus change upon liquefaction, movement of the stress path towards zero mean effective stress may be better replicated. In line with this suggestion, a smaller plastic modulus will provide a softer response, which has been observed experimentally. However, introduction of a new method in predicting pore pressure generation for the post-liquefaction phase requires especial attention to dynamic loads.

In conclusion, the proposed constitutive model in its current shape is valid for predicting drained and undrained triaxial cyclic response of sand under both compression and extension conditions. The predictive capability of the model for post-liquefaction phase under undrained condition, however, is not promising. Therefore, some modifications in the model formulation are required in order to enhance the model ability in reproducing the post-liquefaction response. To extend the application of the proposed constitutive model, it should be further validated against non-triaxial tests such as simple shear test or hollow cylinder test conditions.

Acknowledgement

The authors would like to acknowledge the research funding for this study provided by NSERC through a Collaborative Research Development program supported by BP Canada.

References

- Al-Tabbaa, A. (1987), Permeability And Stress-Strain Response of Speswhite Kaolin, PhD thesis, The University of Cambridge.
- Araujo, M.C. (2002), Non-linear kinematic hardening model for multiaxial cyclic plasticity, M.Sc. thesis, Louisiana State University, Louisiana, USA.
- Armstrong, P.J. and Frederick, C.O. (1966), A mathematical representation of the multiaxial Bauschinger effect, CEGB Report, RD/B/N731, Berkeley Nuclear Laboratories.
- Bardet, J.P. (1986), Bounding Surface Plasticity Model For Sands, Journal of Engineering Mechanics, Vol. 112, No. 11, pp. 1198-1217.
- Been, K., and Jefferies, M. G. (1985), A state parameter for sands, Geotechnique, Vol. 35, No. 2, pp. 99-112.
- Chen, W.F. (1994), Constitutive Equations for Engineering Materials, Elsevier, Netherland.
- Chen, W.F. and Han D.J. (2007), Plasticity for Structural Engineers, John Ross Publishing, USA.
- Crouch, R.S., Wolf, J.P., and Dafalias, Y.F. (1994), Unified Critical-State Bounding-Surface Plasticity Model For Soils, Journal of Engineering Mechanics, Vol. 120, No. 11, pp. 2251-2270.
- Dafalias, Y.F. (1986), Bounding Surface Plasticity. I: Mathematical Foundation And Hypoplasticity, Journal of Engineering Mechanics, Vol. 112, No. 9, pp. 966-987.
- Dafalias, Y.F., and Herrmann, L.R. (1982), Bounding surface formulation of soil plasticity, Soil Mechanics-Transient and Cyclic Loads, Wiley, pp. 253-282.
- Dafalias, Y.F., and Popov, E.P. (1975), A Model of Nonlinearly Hardening Materials for Complex Loading, Acta Mechanica, Vol. 21, pp. 173-192.
- Dafalias, Y.F., and Popov, E.P. (1977), Cyclic Loading For Materials With A Vanishing Elastic Region, Nuclear Energy and Design, Vol. 41, pp. 293-302.
- Dunne, F., and Petrinic, N. (2006), Introduction to computational plasticity, Oxford University Press, USA.
- Elgamal, A., Yang, Z., Parra, E. and Regheb, A. (2003), Modeling of Cyclic Mobility in Saturated Cohesionless Soils, International Journal of Plasticity, Vol. 19, pp. 883-905.
- Habte, M.A. (2006), Numerical and constitutive modelling of monotonic and cyclic loading in variably saturated soils, PhD thesis, The University of New South Wales.

- Imam, M.R. (1999), Modeling the constitutive behavior of sand for the analysis of static liquefaction, PhD thesis, The University of Alberta.
- Imam, M.R., and Chan, D.H. (2008), Application of a critical state model for the cyclic loading of sands, *GeoEdmonton*, pp. 127-134.
- Imam, M.R., Morgenstern, N.R., Robertson, P.K., and Chan, D.H. (2002), Yielding and flow liquefaction of loose sand, *Soils and Foundations*. Vol. 42, No. 3, pp. 19-31.
- Imam, M.R., Morgenstern N.R., Robertson P.K., and Chan, D.H. (2005), A critical-state constitutive model for liquefiable sand, *Canadian Geotechnical Journal*, Vol. 42, No. 3, pp. 830-855.
- Ishihara, K. (1993) Liquefaction and flow failure during earthquake. *Geotechnique*, Vol. 43, No. 3, pp. 351-415.
- Ishihara, K., Tatsuoka, F., and Yasuda, S. (1975), Undrained deformation and liquefaction of sand under cyclic stresses, *Soils and Foundation*, Vol. 15. No. 1, pp. 29-44.
- Iwan, W.D. (1967), On a class of models for the yielding behaviour of continuous and composite systems, *Journal of Applied Mechanics*, Vol. 34, pp. 612-617.
- Jefferies, M.G. (1993), Nor-Sand: a simple critical state model for sand, *Geotechnique*, Vol. 43, No. 1, pp. 91-103.
- Kan, M. E, Taiebat, H.A., and Khalili, N. (2014), Simplified mapping rule for bounding surface simulation of complex loading paths in granular materials, *International journal of Geomechanics*, Vol. 14, No. 2, pp. 239-253.
- Khalili, N., Habte, M. A., and Valliappan S. (2005), A bounding surface plasticity model for cyclic loading of granular soils, *International Journal For Numerical Methods In Engineering*, Vol. 63, pp. 1939–1960.
- Khong, CD. (2004), Development and numerical evaluation of unified critical state models, PhD thesis, The University of Nottingham.
- Krieg, R.D. (1975), A practical two-surface plasticity theory, *Journal of Applied Mechanics*, Vol. 42, No. 3, pp. 641-646
- Lenart, S. (2008), The Response of Saturated Soils to a Dynamic Load, *Acta Geotechnica Slovenica*, Vol. 5, No. 1, pp. 37-49.
- Ling, H.I., and Yang, Y. (2006), Unified Sand Model Based on the Critical State and Generalized Plasticity, *Journal of Engineering Mechanics*, Vol. 132, No. 12, pp. 1380-1391.

- Ling, H.I., Yue, D., Kaliakin, V.N., and Themelis, N.J. (2002), Anisotropic Elastoplastic Bounding Surface Model for Cohesive Soils, *Journal of Engineering Mechanics*, Vol. 128, No. 7, pp. 748-758.
- Li, X.S., Ming, H.Y.(2000), Unified modeling of flow liquefaction and cyclic mobility, *Soil Dynamics and Earthquake Engineering*, Vol. 19, pp. 363-369.
- Manzari, M.T., and Dafalias, Y. F. (1997), A critical state two-surface plasticity model for sands, *Geotechnique*, Vol. 47, No. 2, pp. 255-272.
- McDowell G.R., and Hau K.W. (2004), A generalised modified Cam clay model for clay and sand incorporating kinematic hardening and bounding surface plasticity, *Granular Matter*, Springer-Verlag, pp. 11-16.
- Mroz, Z., (1967), "On the description of anisotropic hardening", *Journal of the Mechanics and Physics of Solids*, Vol. 15, pp. 163-175.
- Mroz, Z., NORRIS, V. A. and Zienkiewicz, O.C. (1979), Application of an anisotropic hardening model in the analysis of elasto-plastic deformation of soils, *Geotechnique*, Vol. 29, No. 1, pp. 1-34.
- Orense, R., and Pender M. (2012), Liquefaction Characteristics of Pumice Sands, EQC project 10/589, The University of Auckland.
- Pastor, M., Zienkiewicz, O.C., and Leung, K.K. (1985), Simple model for transient soil loading in models for sands earthquake analysis. II. Non-associated models for sands, *International Journal for Numerical and Analytical Methods in Geomechanics*, Vol. 9, pp. 477-498.
- Pradhan, T. B. S. (1989), The behavior of sand subjected to monotonic and cyclic loadings, PhD thesis, Kyoto University.
- Pradhan, T.B.S., Tatsuoka, F., and Sato, Y. (1989), Experimental stress-dilatancy relations of sand subjected to cyclic loading, *Soild and Foundations*, Vol. 29, pp. 45-64.
- Querol, S.L., and Blázquez, R. (2006), Liquefaction and cyclic mobility model for saturated granular media, *International Journal for Numerical and Analytical Methods in Geomechanics*, Vol.30, pp. 413-439.
- Reilly, M.P.O, and Brown, S.F. (1991), *Cyclic loading of soils: from theory to design*, Blackie and son limited, UK.
- Russel, A., and Khalili N. (2004), A bounding surface plasticity model for sands exhibiting particle crushing, *Canadian Geotechnical Journal*, Vol. 41, No. 6, pp. 1179-1192.
- Stallebrass, S. E. (1990), Modeling the effect of recent stress history on the deformation of overconsolidated soils, Ph.D. thesis, The City University, London, U.K.

- Suebsuk, J., Horpibulsuk, S., and Liu, M.D. (2011), A critical state model for overconsolidated structured clays, *Computers and Geotechnics*, Vol. 38, No. 5, pp. 648-658.
- Tatsuoka, F., and Ishihara, K. (1974), Drained deformation of sand under cyclic stresses reversing direction, *Soils and Foundations*, Vol. 14, No. 3, pp. 51-65.
- Vermeer, P.A., and de Borst, R. (1984), Non-associated plasticity for soils, concrete and rocks, *Heron*, Vol. 29, No. 3, pp. 1-64.
- Wood, D.M. (1990), *Soil Behavior and Critical State Soil Mechanics*, Cambridge University Press, USA.
- Yang, C., Cui, Y.J., Pereira, J.M., and Huang, M.S. (2008), A constitutive model for unsaturated cemented soils under cyclic loading, *Computer and Geotechnics*, Vol. 35, pp. 853-859.
- Yang, C., Huang, M.S., and Cui, Y.J. (2011), Constitutive model of unsaturated structured soils under cyclic loading, Taylor & Francis group, pp. 987-992.
- Yu, H.S. (2006), *Plasticity and Geotechnics*, Springer, USA.
- Yu, H.S., Khong, C., and Wang J. (2007), A unified plasticity model for cyclic behaviour of clay and sand, *Mechanics Research Communications*, Vol. 34, No. 2, pp. 97-114.
- Zienkiewicz, O.C., Leung, K.K., and Pastor, M. (1985), Simple model for transient soil loading in earthquake analysis. I. basic model and its application, *International Journal for Numerical and Analytical Methods in Geomechanics*, Vol. 9, pp. 453-476.